Measurement of χ_{cj} decaying into pn[over ¯]π^{-} and pn[over ¯]π^{-}π^{0}

M. Ablikim *et al.* (BESIII Collaboration)

Phys. Rev. D **86**, 052011 — Published 26 September 2012

DOI: 10.1103/PhysRevD.86.052011

Measurement of χ_{cJ} decaying into $p\bar{n}\pi^-$ and $p\bar{n}\pi^-\pi^0$

M. Ablikim[1], M. N. Achasov[5], O. Albayrak[3], D. J. Ambrose[39], F. F. An[1], Q. An[40], J. Z. Bai[1], Y. Ban[27], J. Becker[2], J. V. Bennett[17], M. Bertani[18A], J. M. Bian[38], E. Boger[20,a], O. Bondarenko[21], I. Boyko[20], R. A. Briere[3], V. Bytev[20], X. Cai[1], O. Cakir[35A], A. Calcaterra[18A], G. F. Cao[1], S. A. Cetin[35B], J. F. Chang[1], G. Chelkov[20,a], G. Chen[1], H. S. Chen[1], J. C. Chen[1], M. L. Chen[1], S. J. Chen[25], X. Chen[27], Y. B. Chen[1], H. P. Cheng[14], Y. P. Chu[1], D. Cronin-Hennessy[38], H. L. Dai[1], J. P. Dai[1], D. Dedovich[20], Z. Y. Deng[1], A. Denig[19], I. Denysenko[20,b], M. Destefanis[43A,43C], W. M. Ding[29], Y. Ding[23], L. Y. Dong[1], M. Y. Dong[1], S. X. Du[46], J. Fang[1], S. S. Fang[1], L. Fava[43B,43C], F. Feldbauer[2], C. Q. Feng[40], R. B. Ferroli[18A], C. D. Fu[1], J. L. Fu[25], Y. Gao[34], C. Geng[40], K. Goetzen[7], W. X. Gong[1], W. Gradl[19], M. Greco[43A,43C], M. H. Gu[1], Y. T. Gu[9], Y. H. Guan[6], A. Q. Guo[26], L. B. Guo[24], Y. P. Guo[26], Y. L. Han[1], F. A. Harris[37], K. L. He[1], M. He[1], Z. Y. He[26], T. Held[2], Y. K. Heng[1], Z. L. Hou[1], H. M. Hu[1], T. Hu[1], G. M. Huang[15], G. S. Huang[40], J. S. Huang[12], X. T. Huang[29], Y. P. Huang[1], T. Hussain[42], C. S. Ji[40], Q. Ji[1], Q. P. Ji[26,c], X. B. Ji[1], X. L. Ji[1], L. L. Jiang[1], X. S. Jiang[1], J. B. Jiao[29], Z. Jiao[14], D. P. Jin[1], S. Jin[1], F. F. Jing[34], N. Kalantar-Nayestanaki[21], M. Kavatsyuk[21], W. Kuehn[36], W. Lai[1], J. S. Lange[36], C. H. Li[1], Cheng Li[40], Cui Li[40], D. M. Li[46], F. Li[1], G. Li[1], H. B. Li[1], J. C. Li[1], K. Li[10], Lei Li[1], Q. J. Li[1], S. L. Li[1], W. D. Li[1], W. G. Li[1], X. L. Li[29], X. N. Li[1], X. Q. Li[26], X. R. Li[28], Z. B. Li[33], H. Liang[40], Y. F. Liang[31], Y. T. Liang[36], G. R. Liao[34], X. T. Liao[1], B. J. Liu[1], C. L. Liu[3], C. X. Liu[1], C. Y. Liu[1], F. H. Liu[30], Fang Liu[1], Feng Liu[15], H. Liu[1], H. H. Liu[13], H. M. Liu[1], H. W. Liu[1], J. P. Liu[44], K. Y. Liu[23], Kai Liu[6], P. L. Liu[29], Q. Liu[6], S. B. Liu[40], X. Liu[22], Y. B. Liu[26], Z. A. Liu[1], Zhiqiang Liu[1], Zhiqing Liu[1], H. Loehner[21], G. R. Lu[12], H. J. Lu[14], J. G. Lu[1], Q. W. Lu[30], X. R. Lu[6], Y. P. Lu[1], C. L. Luo[24], M. X. Luo[45], T. Luo[37], X. L. Luo[1], M. Lv[1], C. L. Ma[6], F. C. Ma[23], H. L. Ma[1], Q. M. Ma[1], S. Ma[1], T. Ma[1], X. Y. Ma[1], Y. Ma[11], F. E. Maas[11], M. Maggiora[43A,43C], Q. A. Malik[42], Y. J. Mao[27], Z. P. Mao[1], J. G. Messchendorp[21], J. Min[1], T. J. Min[1], R. E. Mitchell[17], X. H. Mo[1], C. Morales Morales[11], C. Motzko[2], N. Yu. Muchnoi[5], H. Muramatsu[39], Y. Nefedov[20], C. Nicholson[6], I. B. Nikolaev[5], Z. Ning[1], S. L. Olsen[28], Q. Ouyang[1], S. Pacetti[18B], J. W. Park[28], M. Pelizaeus[37], H. P. Peng[40], K. Peters[7], J. L. Ping[24], R. G. Ping[1], R. Poling[38], E. Prencipe[19], M. Qi[25], S. Qian[1], C. F. Qiao[6], X. S. Qin[1], Y. Qin[27], Z. H. Qin[1], J. F. Qiu[1], K. H. Rashid[42], G. Rong[1], X. D. Ruan[9], A. Sarantsev[20,d], B. D. Schaefer[17], J. Schulze[2], M. Shao[40], C. P. Shen[37,e], X. Y. Shen[1], H. Y. Sheng[1], M. R. Shepherd[17], X. Y. Song[1], S. Spataro[43A,43C], B. Spruck[36], D. H. Sun[1], G. X. Sun[1], J. F. Sun[12], S. S. Sun[1], Y. J. Sun[40], Y. Z. Sun[1], Z. J. Sun[1], Z. T. Sun[40], C. J. Tang[31], X. Tang[1], I. Tapan[35C], E. H. Thorndike[39], D. Toth[38], M. Ullrich[36], G. S. Varner[37], B. Wang[9], B. Q. Wang[27], D. Wang[27], D. Y. Wang[27], K. Wang[1], L. L. Wang[1], L. S. Wang[1], M. Wang[29], P. Wang[1], P. L. Wang[1], Q. Wang[1], Q. J. Wang[1], S. G. Wang[27], X. L. Wang[40], Y. D. Wang[40], Y. F. Wang[1], Y. Q. Wang[29], Z. Wang[1], Z. G. Wang[1], Z. Y. Wang[1], D. H. Wei[8], J. B. Wei[27], P. Weidenkaff[19], Q. G. Wen[40], S. P. Wen[1], M. Werner[36], U. Wiedner[2], L. H. Wu[1], N. Wu[1], S. X. Wu[40], W. Wu[26], Z. Wu[1], L. G. Xia[34], Z. J. Xiao[24], Y. G. Xie[1], Q. L. Xiu[1], G. F. Xu[1], G. M. Xu[27], H. Xu[1], Q. J. Xu[10], X. P. Xu[32], Z. R. Xu[40], F. Xue[15], Z. Xue[1], L. Yan[40], W. B. Yan[40], Y. H. Yan[16], H. X. Yang[1], Y. Yang[15], Y. X. Yang[8], H. Ye[1], M. Ye[1], M. H. Ye[4], B. X. Yu[1], C. X. Yu[26], H. W. Yu[27], J. S. Yu[22], S. P. Yu[29], C. Z. Yuan[1], Y. Yuan[1], A. A. Zafar[42], A. Zallo[18A], Y. Zeng[16], B. X. Zhang[1], B. Y. Zhang[1], C. Zhang[25], C. C. Zhang[1], D. H. Zhang[1], H. H. Zhang[33], H. Y. Zhang[1], J. Q. Zhang[1], J. W. Zhang[1], J. Y. Zhang[1], J. Z. Zhang[1], S. H. Zhang[1], X. J. Zhang[1], X. Y. Zhang[29], Y. Zhang[1], Y. H. Zhang[1], Y. S. Zhang[9], Z. P. Zhang[40], Z. Y. Zhang[44], G. Zhao[1], H. S. Zhao[1], J. W. Zhao[1], K. X. Zhao[24], Lei Zhao[40], Ling Zhao[1], M. G. Zhao[26], Q. Zhao[1], Q. Z. Zhao[9,f], S. J. Zhao[46], T. C. Zhao[1], X. H. Zhao[25], Y. B. Zhao[1], Z. G. Zhao[40], A. Zhemchugov[20,a], B. Zheng[41], J. P. Zheng[1], Y. H. Zheng[6], B. Zhong[1], J. Zhong[2], Z. Zhong[9,f], L. Zhou[1], X. K. Zhou[6], X. R. Zhou[40], C. Zhu[1], K. Zhu[1], K. J. Zhu[1], S. H. Zhu[1], X. L. Zhu[34], Y. C. Zhu[40], Y. M. Zhu[26], Y. S. Zhu[1], Z. A. Zhu[1], J. Zhuang[1], B. S. Zou[1], J. H. Zou[1]

(BESIII Collaboration)

[1] *Institute of High Energy Physics, Beijing 100049, P. R. China*
[2] *Bochum Ruhr-University, 44780 Bochum, Germany*
[3] *Carnegie Mellon University, Pittsburgh, PA 15213, USA*
[4] *China Center of Advanced Science and Technology, Beijing 100190, P. R. China*
[5] *G.I. Budker Institute of Nuclear Physics SB RAS (BINP), Novosibirsk 630090, Russia*

[6] Graduate University of Chinese Academy of Sciences, Beijing 100049, P. R. China
[7] GSI Helmholtzcentre for Heavy Ion Research GmbH, D-64291 Darmstadt, Germany
[8] Guangxi Normal University, Guilin 541004, P. R. China
[9] GuangXi University, Nanning 530004,P.R.China
[10] Hangzhou Normal University, Hangzhou 310036, P. R. China
[11] Helmholtz Institute Mainz, J.J. Becherweg 45,D 55099 Mainz,Germany
[12] Henan Normal University, Xinxiang 453007, P. R. China
[13] Henan University of Science and Technology, Luoyang 471003, P. R. China
[14] Huangshan College, Huangshan 245000, P. R. China
[15] Huazhong Normal University, Wuhan 430079, P. R. China
[16] Hunan University, Changsha 410082, P. R. China
[17] Indiana University, Bloomington, Indiana 47405, USA
[18] (A)INFN Laboratori Nazionali di Frascati, Frascati, Italy;
(B)INFN and University of Perugia, I-06100, Perugia, Italy
[19] Johannes Gutenberg University of Mainz, Johann-Joachim-Becher-Weg 45, 55099 Mainz, Germany
[20] Joint Institute for Nuclear Research, 141980 Dubna, Russia
[21] KVI/University of Groningen, 9747 AA Groningen, The Netherlands
[22] Lanzhou University, Lanzhou 730000, P. R. China
[23] Liaoning University, Shenyang 110036, P. R. China
[24] Nanjing Normal University, Nanjing 210046, P. R. China
[25] Nanjing University, Nanjing 210093, P. R. China
[26] Nankai University, Tianjin 300071, P. R. China
[27] Peking University, Beijing 100871, P. R. China
[28] Seoul National University, Seoul, 151-747 Korea
[29] Shandong University, Jinan 250100, P. R. China
[30] Shanxi University, Taiyuan 030006, P. R. China
[31] Sichuan University, Chengdu 610064, P. R. China
[32] Soochow University, Suzhou 215006, China
[33] Sun Yat-Sen University, Guangzhou 510275, P. R. China
[34] Tsinghua University, Beijing 100084, P. R. China
[35] (A)Ankara University, Ankara, Turkey; (B)Dogus University,
Istanbul, Turkey; (C)Uludag University, Bursa, Turkey
[36] Universitaet Giessen, 35392 Giessen, Germany
[37] University of Hawaii, Honolulu, Hawaii 96822, USA
[38] University of Minnesota, Minneapolis, MN 55455, USA
[39] University of Rochester, Rochester, New York 14627, USA
[40] University of Science and Technology of China, Hefei 230026, P. R. China
[41] University of South China, Hengyang 421001, P. R. China
[42] University of the Punjab, Lahore-54590, Pakistan
[43] (A)University of Turin, Turin, Italy; (B)University of Eastern Piedmont, Alessandria, Italy; (C)INFN, Turin, Italy
[44] Wuhan University, Wuhan 430072, P. R. China
[45] Zhejiang University, Hangzhou 310027, P. R. China
[46] Zhengzhou University, Zhengzhou 450001, P. R. China

[a] also at the Moscow Institute of Physics and Technology, Moscow, Russia
[b] on leave from the Bogolyubov Institute for Theoretical Physics, Kiev, Ukraine
[c] Nankai University, Tianjin,300071,China
[d] also at the PNPI, Gatchina, Russia
[e] now at Nagoya University, Nagoya, Japan
[f] Guangxi University,Nanning,530004,China

Using a data sample of 1.06×10^8 ψ' events collected with the BESIII detector in 2009, the branching fractions of $\chi_{cJ} \to p\bar{n}\pi^-$ and $\chi_{cJ} \to p\bar{n}\pi^-\pi^0$ (J=0,1,2) are measured[1]. The results for $\chi_{c0} \to p\bar{n}\pi^-$ and $\chi_{c2} \to p\bar{n}\pi^-$ are consistent with, but much more precise than those of previous

measurements. The decays of $\chi_{c1} \to p\bar{n}\pi^-$ and $\chi_{cJ} \to p\bar{n}\pi^-\pi^0$ are observed for the first time.

PACS numbers: 14.20.Gk, 13.75.Gx, 13.25.Gv

I. INTRODUCTION

Exclusive heavy quarkonium decays constitute an important laboratory for investigating perturbative Quantum Chromodynamics (pQCD). Compared to J/ψ and ψ', relatively little is known concerning χ_{cJ} decays [1]. More experimental data on exclusive decays of P-wave charmonia is important for a better understanding of the nature of χ_{cJ} states, as well as testing QCD based calculations. Although these states are not directly produced in e^+e^- collisions, they are produced copiously in radiative decays of ψ', with branching fractions around 9% [1]. The large ψ' data sample taken with the Beijing Spectrometer (BESIII) located at the Beijing Electron-Positron Collider (BEPCII) provides an opportunity for a detailed study of χ_{cJ} decays.

Previous studies indicate that the Color Octet Mechanism (COM) [2], $c\bar{c}g \to 2(q\bar{q})$ could have large effects on the observed decay patterns of these P-wave charmonia states [3–7]. To arrive at a comprehensive understanding about P-wave dynamics, both theoretical predictions employing the COM and new precise experimental measurements for χ_{cJ} many-body final states decays are required.

Also, the decays of χ_{cJ} with baryons in the final states provide an excellent place to investigate the production and decay rates of excited nucleon N^* states, which are a very important source of information for understanding the internal structure of the nucleon [8].

The decays $\chi_{cJ} \to p\bar{n}\pi^-$ and $\chi_{cJ} \to p\bar{n}\pi^-\pi^0$ were studied by the BESII experiment with 14×10^6 ψ' events [9]. Due to limited statistics and the detector performance, only $\chi_{c0} \to p\bar{n}\pi^-$ and $\chi_{c2} \to p\bar{n}\pi^-$ were observed and measured with large uncertainties. A series of three-body and four-body decays of χ_{cJ}, including channels with similar final states to ours such as $p\bar{p}\pi^0$ and $p\bar{p}\pi^0\pi^0$, were measured by the CLEO-c Collaboration [10, 11].

In this paper, we present a measurement of χ_{cJ} decaying into $p\bar{n}\pi^-$ and $p\bar{n}\pi^-\pi^0$. The samples used in this analysis consist of 156.4 pb^{-1} of ψ' data corresponding to $(1.06\pm0.04)\times10^8$ [12] events taken at $\sqrt{s} = 3.686$ GeV/c^2, and 42.6 pb^{-1} of continuum data taken at $\sqrt{s} = 3.65$ GeV/c^2.

II. DETECTOR AND MONTE-CARLO SIMULATION

BESIII [13] is a major upgrade of the BESII experiment at the BEPCII accelerator [14] for studies of hadron spectroscopy as well as τ-charm physics [15]. The design peak luminosity of the double-ring e^+e^- collider, BEPCII, is 10^{33} cm$^{-2}s^{-1}$ at center-of-mass energy of 3.78 GeV. The BESIII detector with a geometrical acceptance of 93% of 4π, consists of the following main components: 1) a small cell, helium-based main draft chamber (MDC) with 43 layers. The average single wire resolution is 135 μm, and the momentum resolution for 1 GeV/c charged particles in a 1 T magnetic field is 0.5%; 2) an electromagnetic calorimeter (EMC) comprised of 6240 CsI (Tl) crystals arranged in a cylindrical shape (barrel) plus two end-caps. For 1.0 GeV/c photons, the energy resolution is 2.5% (5%) and the position resolution is 6 mm (9 mm) in the barrel (end-caps); 3) a Time-Of-Flight system (TOF) for particle identification (PID) composed of a barrel part constructed of two layers with 88 pieces of 5 cm thick, 2.4 m long plastic scintillators in each layer, and two end-caps with 48 fan-shaped, 5 cm thick, plastic scintillators in each end-cap. The time resolution is 80 ps (110 ps) in the barrel (end-caps), corresponding to a K/π separation by more than 2σ for momenta below about 1 GeV/c; 4) a muon chamber system (MUC) consisting of 1000 m^2 of Resistive Plate Chambers (RPC) arranged in 9 layers in the barrel and 8 layers in the end-caps and incorporated in the return iron yoke of the superconducting magnet. The position resolution is about 2 cm.

The optimization of the event selection and the estimation of backgrounds are performed through Monte Carlo (MC) simulation. The GEANT4-based simulation software BOOST [16] includes the geometric and material description of the BESIII detectors and the detector response and digitization models, as well as the tracking of the detector running conditions and performance. The production of the ψ' resonance is simulated by the MC event generator

[1] Throughout the text, inclusion of charge conjugate modes is implied if not stated otherwise.

KKMC [17], while the decays are generated by EVTGEN [18] for known decay modes with branching fractions being set to world average values [1], and by LUNDCHARM [19] for the remaining unknown decays.

III. EVENT SELECTION

Charged-particle tracks in the polar angle range $|\cos\theta|$ <0.93 are reconstructed from hits in the MDC. Only the tracks with the point of closest approach to the beamline within ±5 cm of the interaction point in the beam direction, and within 0.5 cm in the plane perpendicular to the beam are selected. The TOF and dE/dx information are used to form particle identification (PID) confidence levels for π, K and p hypotheses. Each track is assigned to the particle type that corresponds to the hypothesis with the highest confidence level. Exactly one proton and one π^-, or one antiproton and one π^+ in the event are required in the analysis.

Photon candidates are reconstructed by clustering the EMC crystal energies. The minimum energy is 25 MeV for barrel showers ($|\cos\theta| < 0.80$) and 50 MeV for end-cap showers ($0.86 < |\cos\theta| < 0.92$). EMC cluster timing requirements are made to suppress electronic noise and energy deposits unrelated to the events.

A. Selection of $\psi' \to \gamma\chi_{cJ}, \chi_{cJ} \to p\bar{n}\pi^-$

For the channel $\psi' \to \gamma\chi_{cJ}, \chi_{cJ} \to p\bar{n}\pi^-$, at least one photon with energy greater than 80 MeV is required. To remove photons coming from interactions of charged particles or neutrons (antineutrons) in the detector, the angles between the photon and the antiproton, antineutron and other particles (pion, proton and neutron) are required to be greater than 30°, 20°, and 10°, respectively. A one-constraint (1C) kinematic fit is performed under the $\psi' \to \gamma p\bar{n}\pi^-$ hypothesis, where the neutron (antineutron) is treated as a missing particle. For events with more than one isolated photon candidate, the combination with the smallest χ^2_{1C} is retained, and $\chi^2_{1C} < 10$ is required. The distributions of the recoiling mass against $\gamma p\pi^-$ and $\gamma\bar{p}\pi^+$ are shown in Fig. 1 (a) and Fig. 1 (b), respectively. Clear neutron and antineutron peaks are observed around 0.938 GeV/c^2.

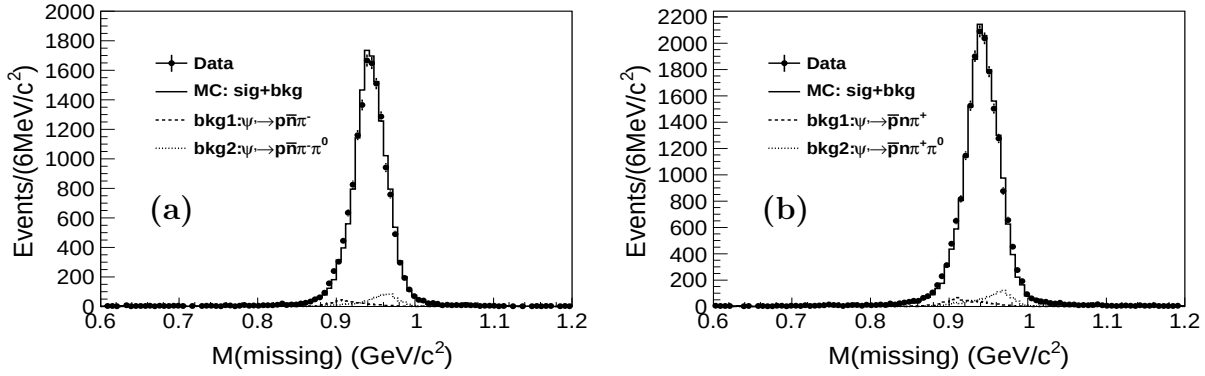

FIG. 1: The distributions of mass recoiling (a) against $\gamma p\pi^-$ in $\psi' \to \gamma p\bar{n}\pi^-$ and (b) against $\gamma\bar{p}\pi^+$ in $\psi' \to \gamma\bar{p}n\pi^+$. Dots with error bars are data, and the solid histograms are the sum of signal and backgrounds, where the backgrounds are estimated from the inclusive MC and the continuum data at $\sqrt{s} = 3.65$ GeV/c^2. The dominant background contributions from $\psi' \to p\bar{n}\pi^-(\bar{p}n\pi^+)$ and $\psi' \to p\bar{n}\pi^-\pi^0$ ($\bar{p}n\pi^+\pi^0$) are shown as dashed and dotted lines, respectively.

An antineutron can form a cluster in the EMC with very high probability due to annihilation in the detector. To further purify the events with antineutrons and more than one photon, $\alpha < 15°$ is required, where α is the angle between the expected antineutron direction and the nearest photon. Further, $M_{p\pi^-(\bar{p}\pi^+)} > 1.15$ GeV/c^2 is required to remove background events with Λ or $\bar{\Lambda}$. Finally, the transverse momentum for the proton or antiproton is required to be greater than 0.3 GeV/c due to the difference of the tracking efficiency at low transverse momentum between data and MC.

B. Selection of $\psi' \to \gamma\chi_{cJ}, \chi_{cJ} \to p\bar{n}\pi^-\pi^0$

For $\psi' \to \gamma\chi_{cJ}, \chi_{cJ} \to p\bar{n}\pi^-\pi^0$, at least three isolated photons are required, where the photon isolation criteria are the same as those in $\psi' \to \gamma\chi_{cJ}, \chi_{cJ} \to p\bar{n}\pi^-$. π^0 candidates are selected from any pair of photon candidates that can be kinematically fitted to the π^0 mass and satisfy $\chi^2 < 20$. There must be at least one π^0 candidate. A 1C kinematic fit is performed to the $\psi' \to \gamma\gamma\gamma p\bar{n}\pi^-$ hypothesis constraining the mass of the missing particle to that of the neutron, where the three photons are a π^0 candidate together with another photon. Kinematic fits are carried out over all possible three-photon combinations. The kinematic fit with the smallest $\chi^2_{\gamma\gamma\gamma p\bar{n}\pi^-}$ is retained, and $\chi^2_{\gamma\gamma\gamma p\bar{n}\pi^-} < 10$ is required. If there is more than one π^0 candidate among the three photons, the pair with the invariant mass closest to the π^0 mass is assigned to be from the π^0 decay. To further suppress backgrounds with final states $\gamma\gamma p\bar{n}\pi^-$ and $\gamma\gamma\gamma\gamma p\bar{n}\pi^-$, 1C kinematic fits are performed under $\gamma\gamma p\bar{n}\pi^-$ and $\gamma\gamma\gamma\gamma p\bar{n}\pi^-$ hypotheses,[1] and $\chi^2_{\gamma\gamma\gamma p\bar{n}\pi^-} < \chi^2_{\gamma\gamma p\bar{n}\pi^-}$ and $\chi^2_{\gamma\gamma\gamma p\bar{n}\pi^-} < \chi^2_{\gamma\gamma\gamma\gamma p\bar{n}\pi^-}$ are required. With the above selection criteria, the invariant mass of π^0 and the distribution of the recoiling mass against $\gamma p\pi^-\pi^0$ in $\psi' \to \gamma p\bar{n}\pi^-\pi^0$ are shown in Fig. 2 (a) and Fig. 2 (b), respectively. Similar distributions are obtained in the charge conjugate channel.

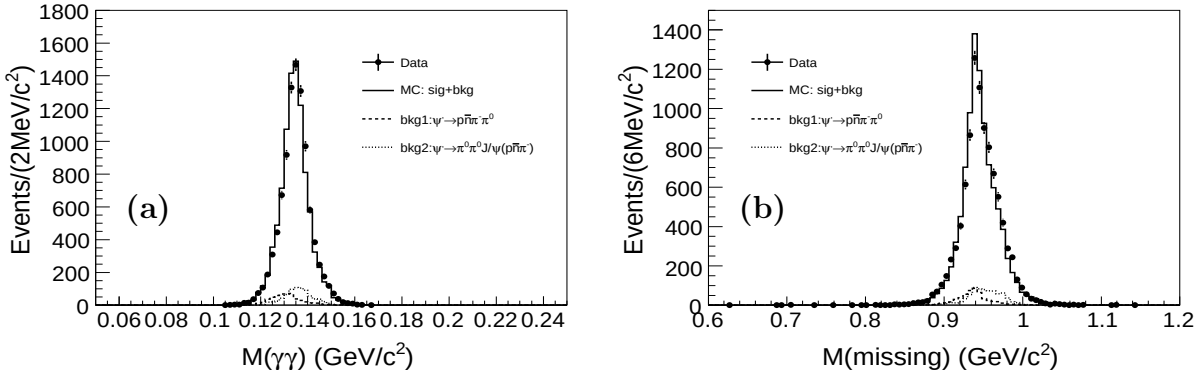

FIG. 2: The invariant mass distribution of (a) $\gamma\gamma$ from π^0 and (b) the distribution of recoiling mass against $\gamma p\pi^-\pi^0$ in $\psi' \to \gamma p\bar{n}\pi^-\pi^0$. Dots with error bars are data, and the solid histograms show the sum of signal and backgrounds, where the backgrounds are estimated from the inclusive MC and the continuum data at $\sqrt{s} = 3.65$ GeV/c^2. The dominant background contributions from $\psi(2S) \to p\bar{n}\pi^-\pi^0$ and $\psi(2S) \to \pi^0\pi^0 J/\psi, J/\psi \to p\bar{n}\pi^-$ are shown as dashed and dotted lines, respectively.

To suppress the background from $\psi' \to \pi^0\pi^0 J/\psi$, for events with at least four photons, $\pi^0\pi^0$ combinations are formed with any four photons, the one with the smallest $\Delta = \sqrt{(m_{\gamma_1\gamma_2} - m_{\pi^0})^2 + (m_{\gamma_3\gamma_4} - m_{\pi^0})^2}$ is selected, and $|M_{recoil} - M_{J/\psi}| > 50$ MeV/c^2 is required, where M_{recoil} is the mass recoiling against $\pi^0\pi^0$. To purify the channel with antineutrons, the same requirement $\alpha < 15^\circ$ as that for the channel $\psi' \to \gamma\chi_{cJ}, \chi_{cJ} \to p\bar{n}\pi^-$ is applied, and the transverse momentum for proton or antiproton is required to be greater than 0.3 GeV/c in order to reduce the systematic uncertainty.

With the above criteria, clear χ_{cJ} signals are observed in the invariant mass distributions of $p\bar{n}\pi^-(\bar{p}n\pi^+)$ in $\chi_{cJ} \to p\bar{n}\pi^-(\bar{p}n\pi^+)$ and of $p\bar{n}\pi^-\pi^0(\bar{p}n\pi^+\pi^0)$ in $\chi_{cJ} \to p\bar{n}\pi^-\pi^0(\bar{p}n\pi^+\pi^0)$, as shown in Figs. 3 (a) and (b) and Figs. 4 (a) and (b), respectively.

IV. BACKGROUND STUDIES

Background is investigated using both exclusive and inclusive MC samples, as well as continuum data. For $\psi' \to \gamma\chi_{cJ}, \chi_{cJ} \to p\bar{n}\pi^-$, a number of individual channels from the inclusive MC sample have been found to contribute to the background. The following reactions have been found to be important: $\psi' \to p\bar{n}\pi^-\pi^0$ ($\approx 20\%$ of the total background), $\psi' \to p\bar{n}\pi^-$ (8%), $\psi' \to \pi^0\pi^0 J/\psi$ with $J/\psi \to p\bar{n}\pi^-$ (1%), and $\psi' \to \gamma\chi_{cJ}$ with $\chi_{cJ} \to p\bar{n}\pi^-\pi^0$ (4%). For the first

[1] The two-photon combinations are pairs of photons from π^0 candidates, and the four-photon combination are pairs of photons from π^0 candidates together with another two photons. If there are multiple combinations, the one with the smallest χ^2 is selected.

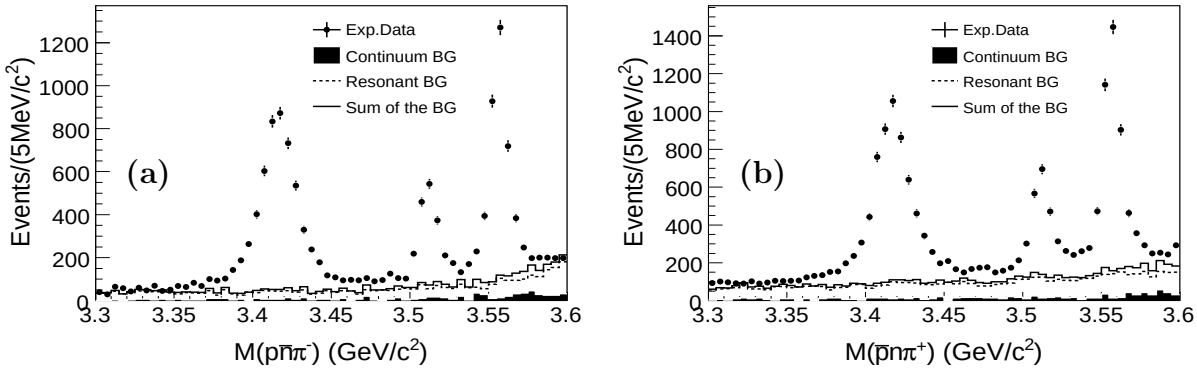

FIG. 3: Invariant mass distribution of (a) $p\bar{n}\pi^-$ for $\psi' \to \gamma p\bar{n}\pi^-$ events, and of (b) $\bar{p}n\pi^+$ for the charge conjugate channel. Dots with error bars are data, and the filled histogram is the normalized non-resonant contribution estimated from continuum data at $\sqrt{s} = 3.65$ GeV/c^2. Resonant background, shown as the dashed histogram, is dominant and is estimated from MC. The sum of both background contributions is shown as the solid histogram.

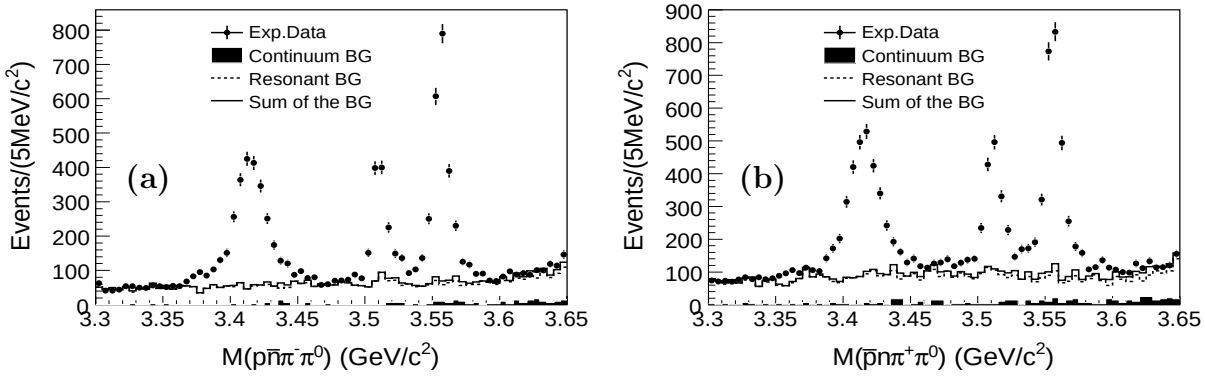

FIG. 4: Invariant mass distribution of (a) $p\bar{n}\pi^-\pi^0$ for the $\psi' \to \gamma p\bar{n}\pi^-\pi^0$ channel, and of (b) $\bar{p}n\pi^+\pi^0$ for the charge conjugate channel. Dots with error bars are data, and the filled histogram is the normalized non-resonant background contribution estimated from continuum data at $\sqrt{s} = 3.65$ GeV/c^2. Resonant background, shown as the dashed histogram, is dominant and is estimated from MC. The sum of both background contributions is shown as the solid histogram.

three background channels, the world average branching fractions listed in PDG [1] are used for normalization, and for $\chi_{cJ} \to p\bar{n}\pi^-\pi^0$, we use our own measurement as described in Sect. VI. The background originating from non-resonant processes is estimated using a continuum data sample collected at a center-of-mass energy of 3.65 GeV/c^2 after normalizing it to the integrated luminosity and the production cross section. The invariant mass distributions of $p\bar{n}\pi^-$ and of the charged conjugate state $\bar{p}n\pi^+$ are shown in Figs. 3 (a) and (b), respectively. No peaking background is observed in the signal region.

Also $\psi' \to \gamma\chi_{cJ}, \chi_{cJ} \to p\bar{n}\pi^-\pi^0$ contains a number of individual background channels according to studies with the inclusive MC sample. The dominant sources are the reactions $\psi' \to p\bar{n}\pi^-\pi^0$ ($\approx 25\%$ of the total background), $\psi' \to \pi^0\pi^0 J/\psi$ with $J/\psi \to p\bar{n}\pi^-$ (10%), and $\psi' \to \gamma\chi_{cJ}$ with $\chi_{cJ} \to p\bar{n}\pi^-$ (1%). Again, for the latter channel the branching fraction obtained from our own measurement is used for normalization (see Sect. VI); for the first two background channels the PDG [1] branching fractions are used. Additional background is studied using the inclusive MC sample, and the continuum data sample. The invariant mass distributions of $p\bar{n}\pi^-\pi^0$ and $\bar{p}n\pi^+\pi^0$ are shown in Fig. 4 (a) and Fig. 4 (b), respectively. Also in this case, no peaking background is observed in the signal region. It has been explicitly verified that the process $\psi' \to \gamma\chi_{cJ}, \chi_{cJ} \to \gamma J/\psi$ with $J/\psi \to p\bar{n}\pi^-$ or $J/\psi \to p\bar{n}\pi^-\pi^0$ does not represent a significant source of background.

V. INTERMEDIATE STATES

We have searched for potential intermediate N^* baryon resonances decaying into either $p\pi^-$ or $\bar{n}\pi^-$. Such a study is needed for correct modeling of $\chi_{cJ} \to p\bar{n}\pi^-$ and $\chi_{cJ} \to p\bar{n}\pi^-\pi^0$ in order to determine the efficiencies used in the calculation of the branching fractions of these decays, which is the main purpose of this work. Selecting χ_{c0} events in the $p\bar{n}\pi^-$ decay mode, $|M_{p\bar{n}\pi^-} - M_{\chi_{c0}}| < 45$ MeV/c^2, the efficiency corrected $p\pi^-$ and $\bar{n}\pi^-$ invariant mass distributions are shown in Fig. 5 (a) and Fig. 5 (b), respectively. Background contributions are also shown and are obtained from the sideband invariant mass region 45 MeV/c^2 $< |M_{p\bar{n}\pi^-} - M_{\chi_{c0}}| <$ 75 MeV/c^2. Fig. 5 (d) shows in addition the corresponding Dalitz plot $M^2(\bar{n}\pi^-)$ vs. $M^2(p\pi^-)$. The structures of the N^* states at around 1.4 GeV/c^2 and 1.7 GeV/c^2 can be seen in both the $p\pi^-$ and $\bar{n}\pi^-$ invariant mass spectra as well as the bands in the Dalitz plot. The $p\bar{n}$ invariant mass is shown in Fig. 5 (c). A large enhancement in the $p\bar{n}$ threshold region is observed, which is also visible as a diagonal band along the upper right-band edge in the Dalitz plot in Fig. 5 (d). A similar threshold enhancement has qualitatively been observed elsewhere, such as a $p\bar{p}$ threshold enhancement in B meson decays [20–25], ψ' decays [26], and in the shape of the timelike electromagnetic form factor of the proton measured at BaBar [27].

The peak at around 2.2 GeV/c^2 in both the $p\pi^-$ and $\bar{n}\pi^-$ invariant mass spectra is partly due to the reflection of the threshold enhancement of $p\bar{n}$. It might also be partly due to high mass N^* states, such as $N^*(2190)$ or $N^*(2220)$. The same structures are observed in the charge conjugate mode of $\chi_{c0} \to \bar{p}n\pi^+$ and the decays of $\chi_{c1,2} \to p\bar{n}\pi^-$. A partial wave analysis is necessary to obtain more information about the N^* components and the threshold enhancement in the invariant mass distribution of $p\bar{n}$.

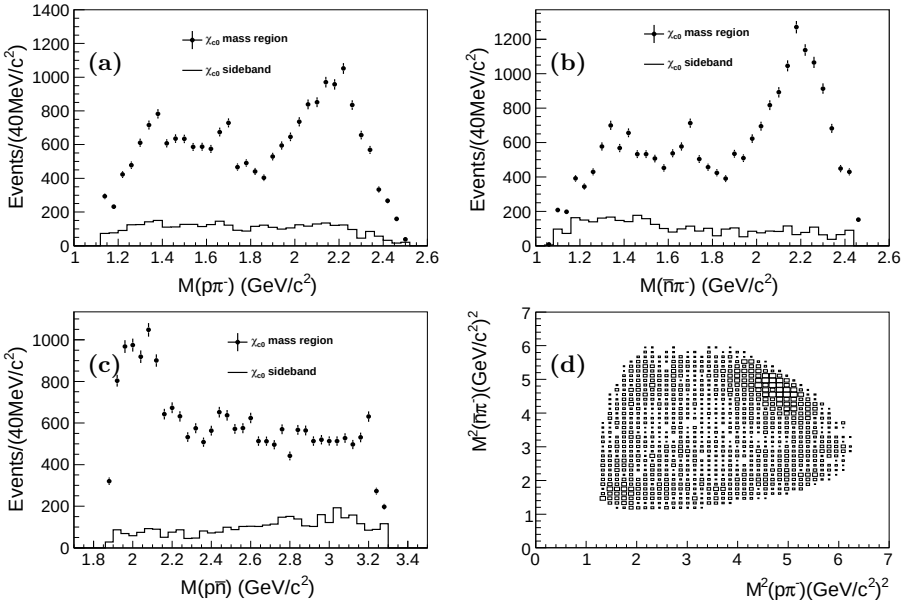

FIG. 5: The invariant mass distributions with the efficiency correction of (a) $p\pi^-$, (b) $\bar{n}\pi^-$, (c) $p\bar{n}$ and (d) Dalitz plot for $\chi_{c0} \to p\bar{n}\pi^-$ events. The dots with error bars are data, and the histograms are for backgrounds obtained from sideband events.

In $\chi_{cJ} \to p\bar{n}\pi^-\pi^0$, various two-body and three-body invariant mass distributions for events within the χ_{cJ} signal region were investigated as well. No obvious N^* state is observed. The distributions are very similar to those of phase space, except the $\pi^\pm\pi^0$ invariant mass spectra that show a significant $\rho^\pm$ signal (see Fig. 6).

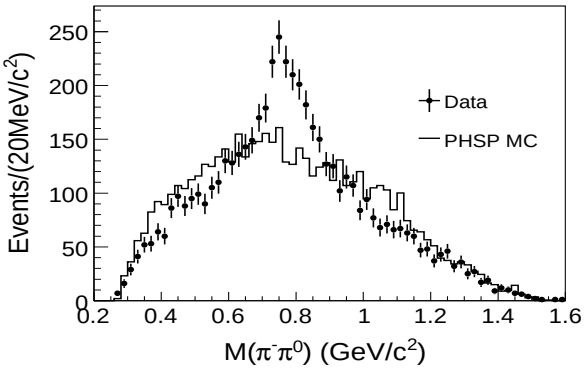

FIG. 6: The invariant $\pi^-\pi^0$ mass distribution in $\chi_{cJ} \to p\bar{n}\pi^-\pi^0$ where a significant ρ signal is observed in the data.

VI. SIGNAL EXTRACTION

Signal yields are extracted using unbinned maximum likelihood fits to the observed $p\bar{n}\pi^-$ and the $p\bar{n}\pi^-\pi^0$ invariant mass distributions. The following formula has been used for the fit:

$$\sum_{i=0}^{2} BW(m; M_i; \Gamma_i) \otimes G(m; \sigma_i) + BG, \tag{1}$$

where $BW(m; M_i;\ \Gamma_i)$ is the Breit-Wigner function for the natural lineshape of the χ_{cJ} resonance, BG represents the background shape and is described by a third order Chebychev polynomial, and G(m; σ_i) is a modified Gaussian function parameterizing the instrumental mass resolution, which was used by ZEUS Collaboration in ref [28] and expressed by:

$$G(m; \sigma_i) = \frac{1}{\sqrt{2\pi}\sigma_i} e^{-(|\frac{m}{\sigma_i}|)^{1+(\frac{1}{1+|\frac{m}{\sigma_i}|})}}. \tag{2}$$

In the fit, the natural widths of the χ_{cJ} states are fixed to the PDG [1] values, while their masses and corresponding instrumental resolutions are floated. For $\psi' \to \gamma\chi_{cJ}, \chi_{cJ} \to p\bar{n}\pi^-$, this fit is performed in the mass region of 3.30 GeV/$c^2 \leq M(p\bar{n}\pi^-) \leq$ 3.60 GeV/c^2, for the process $\psi' \to \gamma\chi_{cJ}, \chi_{cJ} \to p\bar{n}\pi^-\pi^0$ the mass region of 3.30 GeV/$c^2 \leq$ 3.64 GeV/c^2 has been chosen.

The fits to the $p\bar{n}\pi^-$ and $\bar{p}n\pi^+$ invariant mass distributions are shown in Fig. 7 (a) and 7 (b), respectively. The corresponding fits to the $p\bar{n}\pi^-\pi^0$ and $\bar{p}n\pi^+\pi^0$ invariant mass distributions are shown in Figs. 8 (a) and (b), respectively.

MC samples for signal events have been generated to obtain the relevant detection efficiencies. In the underlying event generators, for the decay $\psi' \to \gamma\chi_{cJ}$ an angular distribution proportional to $1+\lambda\cos^2(\theta)$ has been assumed, where θ is the angle between the direction of the radiative photon and the positron beam, and λ = 1, -1/3, 1/13 for J = 0, 1, 2, respectively, in accordance with expectations of electric dipole (E1) transitions. Since in the case of $\psi' \to \gamma\chi_{cJ}, \chi_{cJ} \to p\bar{n}\pi^-$, structures have been observed in the $p\pi^-$, $\bar{n}\pi^-$, and $p\bar{n}$ invariant mass spectra (see Sect. V), the decays of χ_{cJ} into $p\bar{n}\pi^-$ are generated taking these structures and the polar angle distribution of the proton/neutron into account. The MC samples of $\chi_{cJ} \to p\bar{n}\pi^-\pi^0$ used to determine the detection efficiencies were generated with a flat angular distribution, although a $\rho^\pm$ intermediate state is seen. To estimate the systematic uncertainty associated with the missing $\rho^\pm$ intermediate state, a MC production of $\chi_{cJ} \to p\bar{n}\rho^-$ with the correct angular distribution of $\rho^\pm \to \pi^\pm\pi^0$ has been generated (see Sect. VIII).

The χ_{c0}, χ_{c1} and χ_{c2} MC samples are finally weighted with the amplitudes observed in data, and the same fitting process as that for data is performed to the mixed MC sample. The detection efficiencies of χ_{cJ} are calculated by $\varepsilon_{cJ} = N_{cJ}^{fit}/N_{cJ}^{gen}$, where N_{cJ}^{fit} is the number of χ_{cJ} events extracted from the fit, and N_{cJ}^{gen} is the number of generated χ_{cJ} events.

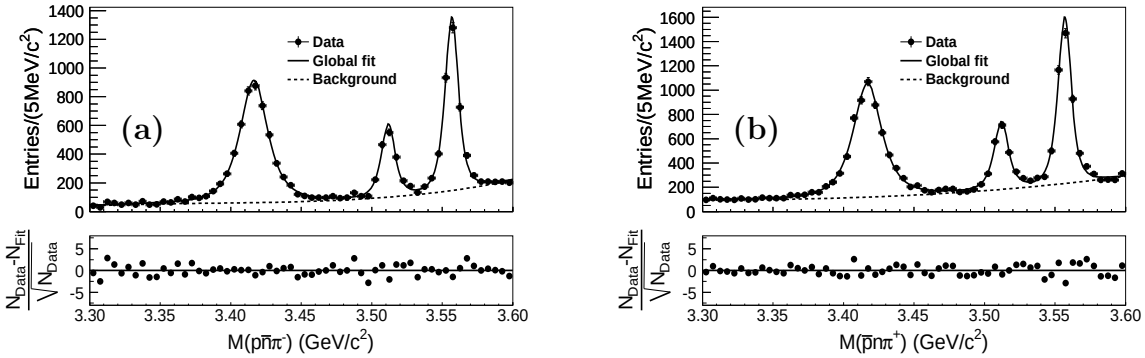

FIG. 7: Upper plot: The fit to the invariant mass distributions of (a) $p\bar{n}\pi^-$ and (b) the charge conjugate state $\bar{p}n\pi^+$. Dots with error bars are data, the solid curve is showing the fit to signal events, and the dashed line is the fitted background distribution. Lower plot: The distribution of $\frac{N_{Data}-N_{Fit}}{\sqrt{N_{Data}}}$ from the fit.

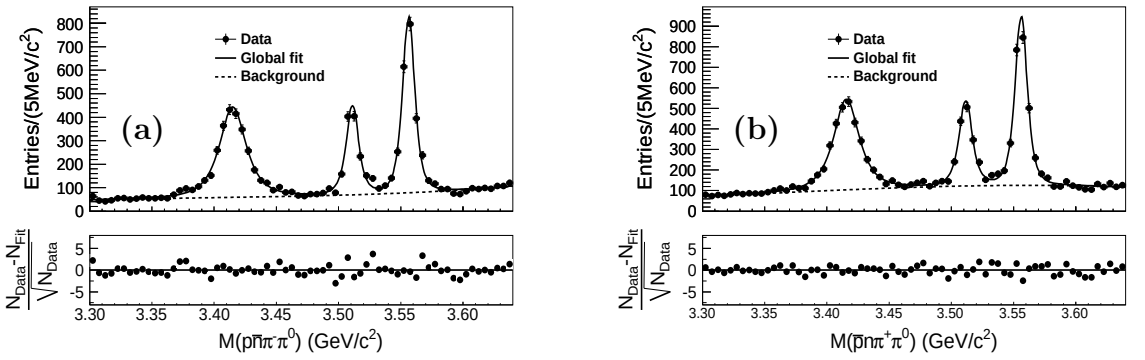

FIG. 8: Upper plot: The fit to the invariant mass distributions of (a) $p\bar{n}\pi^-\pi^0$ and (b) the charge conjugate state $\bar{p}n\pi^+\pi^0$. Dots with error bars are data, the solid curve is showing the fit to signal events, and the dashed line is the fitted background distribution. Lower plot: The distribution of $\frac{N_{Data}-N_{Fit}}{\sqrt{N_{Data}}}$ from the fit.

VII. BRANCHING FRACTIONS

A. Branching fractions of $\chi_{cJ} \to p\bar{n}\pi^-$

The branching fractions of $\chi_{cJ} \to p\bar{n}\pi^-$ are calculated according to:

$$\mathcal{B}(\chi_{cJ} \to p\bar{n}\pi^-) = \frac{N_{sig}}{N_{\psi'} \times \mathcal{B}(\psi' \to \gamma\chi_{cJ}) \times \varepsilon_{cJ}}, \tag{3}$$

where N_{sig} is the number of signal events extracted from the fit to the invariant mass distribution, $N_{\psi'}$ is the number of ψ' events, $\mathcal{B}(\psi' \to \gamma\chi_{cJ})$ is the branching fraction of $\psi' \to \gamma\chi_{cJ}$ as quoted in the PDG [1], and ε_{cJ} is the detection efficiency. The results are summarized in the left column in Table I. The same calculation for the charge conjugate channel is performed, and the results are summarized in the right column.

B. Branching fractions of $\chi_{cJ} \to p\bar{n}\pi^-\pi^0$

Considering the branching fraction of $\pi^0 \to \gamma\gamma$, the branching fraction of $\chi_{cJ} \to p\bar{n}\pi^-\pi^0$ is calculated according to:

$$\mathcal{B}(\chi_{cJ} \to p\bar{n}\pi^-\pi^0) = \frac{N_{sig}}{N_{\psi'} \times \mathcal{B}(\psi' \to \gamma\chi_{cJ}) \times \mathcal{B}(\pi^0 \to \gamma\gamma) \times \varepsilon_{cJ}}. \tag{4}$$

TABLE I: The number of signal events N_{sig}, the detection efficiency ε_{cJ}, and the branching fractions of $\chi_{cJ} \to p\bar{n}\pi^-$, where the errors are statistical only.

	$\chi_{cJ} \to p\bar{n}\pi^-$			$\chi_{cJ} \to \bar{p}n\pi^+$		
	χ_{c0}	χ_{c1}	χ_{c2}	χ_{c0}	χ_{c1}	χ_{c2}
N_{sig}	5150±102	1412±58	3309±79	5808±121	1625±73	3732±89
ε_{cJ} (%)	38.6±0.2	35.9±0.3	39.2±0.2	40.9±0.2	40.7±0.3	41.2±0.2
$\mathcal{B}$ (10^{-3})	1.30±0.03	0.40±0.02	0.91±0.02	1.38±0.03	0.41±0.02	0.98±0.02

The results are summarized in the left column in Table II. The corresponding results for the charge conjugate channel are also shown in the right column.

TABLE II: The number of signal events N_{sig}, the detection efficiency ε_{cJ} and the branching fractions of $\chi_{cJ} \to p\bar{n}\pi^-\pi^0$, where the errors are statistical only.

	$\chi_{cJ} \to p\bar{n}\pi^-\pi^0$			$\chi_{cJ} \to \bar{p}n\pi^+\pi^0$		
	χ_{c0}	χ_{c1}	χ_{c2}	χ_{c0}	χ_{c1}	χ_{c2}
N_{sig}	2480±85	1082±52	2128±62	2757±94	1261±60	2352±69
ε_{cJ} (%)	10.4±0.1	10.4±0.2	9.8±0.1	12.2±0.1	12.3±0.2	11.2±0.1
$\mathcal{B}$ (10^{-3})	2.36±0.08	1.08±0.05	2.38±0.07	2.23±0.08	1.06±0.05	2.30±0.07

VIII. ESTIMATION OF SYSTEMATIC UNCERTAINTIES

Several sources of systematic uncertainties are considered in the measurement of the branching fractions. These include differences between data and the MC simulation for the tracking algorithm, the particle identification (PID), photon detection, the kinematic fit, the requirement on the angle α, π^0 reconstruction, the fitting procedure, and the number of ψ' events. Also possible imperfections in the description of intermediate resonances in the MC are considered.

a. Tracking and PID The uncertainties from tracking efficiency and PID are investigated using an almost background-free control sample of $J/\psi \to p\bar{p}\pi^+\pi^-$ from $(225.3 \pm 2.8) \times 10^8$ J/ψ decays [29]. The tracking efficiency is calculated with $\epsilon = N_{full}/N_{all}$, where N_{full} is the number of events with all final tracks reconstructed successfully and N_{all} is the number of events with three of them reconstructed while one track is missing. The PID efficiency is the ratio of the number of selected events with and without PID. Both efficiencies are studied for pions and protons (antiprotons) as a function of transverse momentum and $\cos\theta$. The data - MC simulation difference for the tracking efficiency is estimated to be 1% per track. Therefore, a 2% uncertainty is taken for two-track events. For the PID efficiency, a 2% difference between data and MC is found for antiprotons, and 1% for any other charged particle. Therefore, 2% (3%) is taken as the systematic uncertainty for the final states including $p\pi^-$ ($\bar{p}\pi^+$).

b. Photon detection The uncertainty due to photon detection and photon conversion is 1% per photon. This value is determined from a study using clean control samples, such as $J/\psi \to \rho^0\pi^0$ and $e^+e^- \to \gamma\gamma$. Therefore, a 1% uncertainty is taken for the $\psi' \to \gamma\chi_{cJ} \to \gamma p\bar{n}\pi^-$ channel, while for the $\psi' \to \gamma\chi_{cJ} \to \gamma p\bar{n}\pi^-\pi^0$ channel, with 3 photons in the final state, a 3% uncertainty is taken.

c. Kinematic fit The systematic uncertainty stemming from the 1C kinematic fit is investigated using $J/\psi \to p\bar{n}\pi^-$ and $J/\psi \to p\bar{n}\pi^-\pi^0$ events, where $\bar{n}$ is treated as a missing particle with a mass of 0.938 GeV/c^2. To obtain the systematic uncertainty associated with the fit, pure control samples of $J/\psi \to p\bar{n}\pi^-$ and $J/\psi \to p\bar{n}\pi^-\pi^0$ are selected, and the 1C kinematic fit is applied to both charge states, both for data and MC. The efficiency of the 1C kinematic fit is estimated calculating the ratio of the number of events with and without the kinematic fit. From the two charge conjugate states, the larger difference between data and MC is taken as the systematic uncertainty. We assign an uncertainty of 2.9% for the kinematic fit in the case of $p\bar{n}\pi^-(\pi^0)$ and 2.7% for $\bar{p}n\pi^+(\pi^0)$.

d. Angle α Another source of systematic uncertainty is the requirement on the angle $\alpha_{\gamma\bar{n}} < 15^\circ$. This uncertainty is studied using the $J/\psi \to p\bar{n}\pi^-$ sample and an uncertainty of 1.8% is assigned for this item.

e. π^0 reconstruction The uncertainty from the π^0 reconstruction is determined with a high purity and high statistics sample of $J/\psi \to \pi^+\pi^-\pi^0$. The π^0 selection efficiency is determined by counting the number of π^0 candidates in

the $\pi^+\pi^-$ recoiling mass distribution with and without the standard π^0 selection (1C kinematic fit). The data - MC simulation difference has been measured to be 0.7%, and it has been verified that there is no dependence of this value from the π^0 momentum and π^0 polar angle.

f. Uncertainty from intermediate states As mentioned above, in $\chi_{cJ} \to p\bar{n}\pi^-$, obvious N^* intermediate states and a $p\bar{n}$ threshold enhancement are observed in the invariant mass spectra of $p\pi^-$ ($\bar{n}\pi^-$) and $p\bar{n}$ (Fig. 5). To account for these structures in the determination of the detection efficiency for $\chi_{cJ} \to p\bar{n}\pi^-$, MC samples were produced including these structures at the generator level. To determine the systematic error associated with this procedure, an alternative method is used, where the efficiency, including the effect of these structures for $\chi_{cJ} \to p\bar{n}\pi^-$, is determined by re-weighting MC events generated according to phase space by the ratio of data and MC events in the two-dimensional distribution of $p\pi^-$ versus $\bar{n}\pi^-$ invariant mass. The difference in the detection efficiencies determined by the two methods is assigned as the systematic uncertainty. In $\chi_{cJ} \to p\bar{n}\pi^-\pi^0$, a strong $\rho^\pm$ signal is observed in the $\pi^\pm\pi^0$ invariant mass spectrum (Fig. 6), while MC samples used to estimate the detection efficiencies are generated assuming phase space only. To study the effect of the intermediate state on the efficiencies, a sample of $\chi_{cJ} \to p\bar{n}\rho^-$ events is generated and analyzed. The efficiency difference between the two MC samples with and without a $\rho^\pm$ intermediate state, $(\varepsilon_{pn\pi\pi^0} - \varepsilon_{pn\rho})/\varepsilon_{pn\pi\pi^0}$, is taken as the systematic uncertainty.

g. Fitting procedure As described above, the yields of the χ_{cJ} signal events are derived from fits to the invariant mass spectra of $p\bar{n}\pi^-$ and $p\bar{n}\pi^-\pi^0$. To evaluate the systematic uncertainty associated with the fitting procedure, we have studied the following aspects: (i) *Fitting range:* In the nominal fit, the mass spectra of $p\bar{n}\pi^-$ and $p\bar{n}\pi^-\pi^0$ are fitted from 3.30 GeV/c^2 to 3.60 GeV/c^2 and from 3.30 GeV/c^2 to 3.64 GeV/c^2, respectively. We have changed these intervals to 3.32−3.60 GeV/c^2 in the case of $p\bar{n}\pi^-$ and 3.32−3.62 GeV/c^2 for $p\bar{n}\pi^-\pi^0$ events. The differences in the finally obtained branching fractions by changing the fit intervals, are taken as the systematic uncertainties associated with the fit intervals. (ii) *Signal lineshape:* The partial width for an E1/M1 radiative transition is proportional to the cube of the radiative photon energy (E_γ^3), which leads to a diverging tail in lower mass region. Two damping functions have been proposed by the KEDR [30] and the CLEO [31] collaborations and have been used in addition to the standard approach in the formula describing the fit to the signal lineshape. Differences with respect to the fit not taking into account this damping factor have been observed, and the greater of the two differences is taken as the systematic uncertainty associated with the signal lineshape. (iii) *Mass resolution parameterization:* A single Gaussian formula instead of the modified Gaussian formula (Formula 2) has been used to describe the instrumental mass resolution. The resulting differences for the final branching fractions are taken as the systematic uncertainties. (iv) *Mass resolution:* Studies have shown that the χ_{cJ} mass resolutions, as simulated by MC, are underestimated. To evaluate the systematic effects associated with this aspect, the invariant masses of $p\bar{n}\pi^-$ and $p\bar{n}\pi^-\pi^0$ in the MC samples are smeared with a Gaussian function, where the width of this Gaussian depends on the invariant mass as well as on the channel. The same fitting processes as in the nominal cases are performed on the smeared mass spectra of $p\bar{n}\pi^-$ and $p\bar{n}\pi^-\pi^0$, and the detection efficiencies are recalculated. The efficiency difference between the smeared and unsmeared case is taken as the systematic uncertainty. (v) *Background shape:* To estimate the uncertainties due to the background parameterizations, a second order instead of a third order Chebychev polynomial is applied in the fitting. Again, the difference between the two cases is used as an estimate of the systematic uncertainty.

h. Other systematic uncertainties The number of ψ' events is determined from an inclusive analysis of ψ' hadronic events and an uncertainty of 4% [12] is associated to it. The uncertainties due to the branching fractions of $\psi' \to \gamma\chi_{cJ}$ and $\pi^0 \to \gamma\gamma$ are taken from the PDG [1]. A small uncertainty due to the statistical error of the efficiencies is also considered.

In Table III a summary of all contributions to the systematic error is shown. In each case, the total systematic uncertainty is obtained by adding the individual contributions in quadrature.

IX. SUMMARY

Based on a data sample of 1.06×10^8 ψ' events collected with the BESIII detector, the branching fractions of $\chi_{cJ} \to p\bar{n}\pi^-$ and $\chi_{cJ} \to p\bar{n}\pi^-\pi^0$ are measured for $J = 0, 1, 2$. The results are summarized in Table IV, where for each branching fraction the first error is statistical and the second systematic. The product branching fractions of $\mathcal{B}(\psi' \to \gamma\chi_{cJ}) \times \mathcal{B}(\chi_{cJ} \to p\bar{n}\pi^-)$ and $\mathcal{B}(\psi' \to \gamma\chi_{cJ}) \times \mathcal{B}(\chi_{cJ} \to p\bar{n}\pi^-\pi^0)$ are also summarized in Table V. For $\chi_{c0} \to p\bar{n}\pi^-$ and $\chi_{c2} \to p\bar{n}\pi^-$, the results are consistent with the world average values within one standard deviation, while the precision is improved significantly. For the other χ_{cJ} decay modes, the branching fractions are measured for the first time. A comparison of individual branching fraction shows good agreement between charge conjugate channels. The measurements improve the existing knowledge of the χ_{cJ} states and may provide further insight into

TABLE III: Summary of systematic errors (in %) for the branching fraction measurements of $\chi_{cJ} \to p\bar{n}\pi^-$ and $\chi_{cJ} \to p\bar{n}\pi^-\pi^0$.

	$\chi_{cJ} \to p\bar{n}\pi^-$			$\chi_{cJ} \to \bar{p}n\pi^+$			$\chi_{cJ} \to p\bar{n}\pi^-\pi^0$			$\chi_{cJ} \to \bar{p}n\pi^+\pi^0$		
	χ_{c0}	χ_{c1}	χ_{c2}	χ_{c0}	χ_{c1}	χ_{c2}	χ_{c0}	χ_{c1}	χ_{c2}	χ_{c0}	χ_{c1}	χ_{c2}
MDC tracking	2.0	2.0	2.0	2.0	2.0	2.0	2.0	2.0	2.0	2.0	2.0	2.0
PID	2.0	2.0	2.0	3.0	3.0	3.0	2.0	2.0	2.0	3.0	3.0	3.0
Photon detection	1.0	1.0	1.0	1.0	1.0	1.0	3.0	3.0	3.0	3.0	3.0	3.0
Kinematic fit	2.9	2.9	2.9	2.7	2.7	2.7	2.9	2.9	2.9	2.7	2.7	2.7
$\alpha_{\gamma\bar{n}} < 15^\circ$	1.8	1.8	1.8	-	-	-	1.8	1.8	1.8	-	-	-
π^0 reconstruction	-	-	-	-	-	-	0.7	0.7	0.7	0.7	0.7	0.7
Intermediate states	5.3	6.2	8.2	4.0	1.2	5.0	3.0	1.7	0.7	1.5	1.8	2.3
Fit range	0.3	0.1	0.1	0.6	0.2	0.1	0.0	1.6	1.1	0.4	2.4	0.8
Signal lineshape	1.4	2.4	1.1	0.9	5.4	1.4	0.8	2.5	1.1	1.5	1.7	0.8
Resolution para.	1.9	4.6	3.0	3.1	5.3	3.1	2.1	5.5	1.7	0.4	4.9	2.2
Resolution diff.	0.3	1.4	1.3	0.5	0.2	0.7	1.9	1.9	1.0	0.8	2.4	1.8
Background shape	1.7	5.8	1.2	0.3	1.1	0.2	1.3	1.6	1.1	1.1	2.4	0.9
N(ψ')	4.0	4.0	4.0	4.0	4.0	4.0	4.0	4.0	4.0	4.0	4.0	4.0
$\mathcal{B}(\psi' \to \gamma\chi_{cJ})$	3.2	4.3	3.9	3.2	4.3	3.9	3.2	4.3	3.9	3.2	4.3	3.9
$\mathcal{B}(\pi^0 \to \gamma\gamma)$	-	-	-	-	-	-	0.03	0.03	0.03	0.03	0.03	0.03
MC statistics	0.2	0.3	0.2	0.2	0.3	0.2	0.1	0.2	0.1	0.1	0.2	0.1
Total	9.1	12.5	11.5	8.6	10.8	9.5	8.6	10.6	8.3	7.9	10.6	8.8

their decay mechanisms. Based on the results of this work, detailed studies concerning the intermediate states may follow in the future.

TABLE IV: Summary of branching fractions for $\chi_{cJ} \to p\bar{n}\pi^-$ and $\chi_{cJ} \to p\bar{n}\pi^-\pi^0$. The first errors are statistical, and the second ones are systematic.

	χ_{c0}	χ_{c1}	χ_{c2}
$\mathcal{B}(\chi_{cJ} \to p\bar{n}\pi^-)$ (10^{-3})	1.30±0.03±0.12	0.40±0.02±0.05	0.91±0.02±0.10
$\mathcal{B}(\chi_{cJ} \to \bar{p}n\pi^+)$ (10^{-3})	1.38±0.03±0.12	0.41±0.02±0.04	0.98±0.02±0.09
$\mathcal{B}(\chi_{cJ} \to p\bar{n}\pi^-\pi^0)(10^{-3})$	2.36±0.08±0.20	1.08±0.05±0.12	2.38±0.07±0.20
$\mathcal{B}(\chi_{cJ} \to \bar{p}n\pi^+\pi^0)(10^{-3})$	2.23±0.08±0.18	1.06±0.05±0.11	2.30±0.07±0.20
$\mathcal{B}(\chi_{cJ} \to p\bar{n}\pi^-)$ (10^{-3}) (PDG [1])	1.14±0.31	-	1.10±0.40

TABLE V: Summary of the product branching fractions of $\psi' \to \gamma\chi_{cJ}$, $\chi_{cJ} \to p\bar{n}\pi^-$ and $\psi' \to \gamma\chi_{cJ}$, $\chi_{cJ} \to p\bar{n}\pi^-\pi^0$. The first errors are statistical, and the second ones are systematic.

	χ_{c0}	χ_{c1}	χ_{c2}
$\mathcal{B}(\psi' \to \gamma\chi_{cJ}) \times \mathcal{B}(\chi_{cJ} \to p\bar{n}\pi^-)$ (10^{-4})	1.26±0.02±0.11	0.37±0.02±0.04	0.80±0.02±0.09
$\mathcal{B}(\psi' \to \gamma\chi_{cJ}) \times \mathcal{B}(\chi_{cJ} \to \bar{p}n\pi^+)$ (10^{-4})	1.34±0.03±0.11	0.38±0.02±0.04	0.85±0.02±0.07
$\mathcal{B}(\psi' \to \gamma\chi_{cJ}) \times \mathcal{B}(\chi_{cJ} \to p\bar{n}\pi^-\pi^0)(10^{-4})$	2.29±0.08±0.18	1.00±0.05±0.10	2.07±0.06±0.15
$\mathcal{B}(\psi' \to \gamma\chi_{cJ}) \times \mathcal{B}(\chi_{cJ} \to \bar{p}n\pi^+\pi^0)(10^{-4})$	2.16±0.07±0.16	0.98±0.05±0.10	2.01±0.06±0.16

X. ACKNOWLEDGMENTS

The BESIII collaboration thanks the staff of BEPCII and the computing center for their hard efforts. This work is supported in part by the Ministry of Science and Technology of China under Contract No. 2009CB825200; National Natural Science Foundation of China (NSFC) under Contracts Nos. 10625524, 10821063, 10825524, 10835001,

10875113, 10935007, 11125525, 10979038, 11005109, 11079030; Joint Funds of the National Natural Science Foundation of China under Contracts Nos. 11079008, 11179007; the Chinese Academy of Sciences (CAS) Large-Scale Scientific Facility Program; CAS under Contracts Nos. KJCX2-YW-N29, KJCX2-YW-N45; 100 Talents Program of CAS; Research Fund for the Doctoral Program of Higher Education of China under Contract No. 20093402120022; Istituto Nazionale di Fisica Nucleare, Italy; Ministry of Development of Turkey under Contract No. DPT2006K-120470; U. S. Department of Energy under Contracts Nos. DE-FG02-04ER41291, DE-FG02-91ER40682, DE-FG02-94ER40823; U.S. National Science Foundation, University of Groningen (RuG) and the Helmholtzzentrum fuer Schwerionenforschung GmbH (GSI), Darmstadt; WCU Program of National Research Foundation of Korea under Contract No. R32-2008-000-10155-0.

[1] J. Beringer *et al.* (Particle Data Group), Phys. Rev. D **86**, 010001 (2012).
[2] H. D. Trottier, Phys. Lett. B **320**, 145-151 (1994).
[3] H. W. Huang and K. T. Chao, Phys. Rev. D **54**, 6850 (1996).
[4] A. Petrelli, Phys. Lett B **380**, 159 (1996).
[5] J. Bolz, P. Kroll and G. A. Schuler, Phys. Lett. B **392**, 198 (1997).
[6] S. M. H. Wong, Nucl. Phys. A **674**, 185 (2000).
[7] S. M. H. Wong, Nucl. Phys. Eur. Phys. J. C **14**, 643 (2000).
[8] N. Isgur, arXiv:nucl-th/0007008v1, 6 Jul 2000.
[9] M. Ablikim *et al.* (BES Collaboration), Phys. Rev. D **74**, 012004 (2006).
[10] S. Athar *et al.* (CLEO Collaboration), Phys. Rev. D **75**, 032002 (2007).
[11] Q. He *et al.* (CLEO Collaboration), Phys. Rev. D **78**, 092004 (2008).
[12] M. Ablikim *et al.* (BESIII Collaboration), Phys. Rev. D **81**, 052005 (2010).
[13] M. Ablikim *et al.* (BESIII Collaboration), Nucl. Instrum. Methods Phys. Res., Sect. A **614**, 345 (2010).
[14] J. Z. Bai *et al.* (BESIII Collaboration), Nucl. Instrum. Methods Phys. Res., Sect. A **344**, 319 (1994); **458**, 627(2001).
[15] D. M. Asner *et al.*, Int. J. Mod. Phys. A **24**, No. 1, 499 (2009).
[16] Z. Y. Deng *et al.*, HEP & NP **30**, 371 (2006).
[17] S. Jadach, B. F. L. Ward and Z. Was, Comp. Phys. Commu. **130**, 260 (2000);
S. Jadach, B. F. L. Ward and Z. Was, Phys. Rev. D **63**, 113009 (2001).
[18] R. G. Ping *et al.*, HEP & NP **32**, 599 (2008).
[19] J. C. Chen, G. S. Huang, X. R. Qi, D. H. Zhang, and Y. S. Zhu, Phys. Rev. D **62**, 034003 (2000).
[20] K. Abe *et al.* (Belle Collaboration), Phys. Rev. Lett. **88**, 181803 (2002).
[21] B. Aubert *et al.* (BaBar Collaboration), Phys. Rev. D **72**, 051101(R) (2005).
[22] K. Abe *et al.* (Belle Collaboration), Phys. Rev. Lett. **89**, 151802 (2002).
[23] B. Aubert *et al.* (BaBar Collaboration), Phys. Rev. D **74**, 051101(R) (2006).
[24] J. T. Wei *et al.* (Belle Collaboration), Phys. Lett. B **659**, 80 (2008).
[25] M. Z. Wang *et al.* (Bell Collaboration), Phys. Rev. Lett **92**, 131801 (2004).
[26] J. P. Alexander *et al.* (CLEO Collaboration), Phys. Rev. D **82**, 092002 (2010).
[27] B. Aubert *et al.* (BaBar Collaboration), Phys. Rev. D **73**, 012005 (2006).
[28] S. Chekanov *et al.* (ZEUS Collaboration), Eur. Phys. J. C **44**, 351-366 (2005).
[29] M. Ablikim *et al.* (BESIII Collaboration), arXiv:1207.2865, accepted by Chinese Physics C.
[30] V. V. Anashin *et al.* (KEDR Collaboration), arXiv:hep-ex/1012.1694v1, 8 Dec 2010.
[31] R. E. Mitchell *et al.* (CLEO Collaboration), Phys. Rev. Lett. **102**, 011801 (2009).